JOURNAL OF Applied Polymer SCIENCE

Polyamide 66 Nanocomposites Based on Organoclays Treated with Thermally Stable Phosphonium Salts

Wissam Abdallah, Ulku Yilmazer
Department of Chemical Engineering, Middle East Technical University, 06800 Ankara, Turkey

Correspondence to: U. Yilmazer (E-mail: yilmazer@metu.edu.tr.)

ABSTRACT: Purification of bentonite clays and their modification with two thermally stable (alkyl and aryl) phosphonium organic salts were investigated. The organoclays were subsequently melt compounded with Polyamide 66 (PA66), with and without the use of an elastomeric compatibilizer. The morphology, melt flow, thermal stability, and mechanical properties of the binary and ternary nanocomposites were studied. The bentonite clay was purified by sedimentation, resulting in higher cation exchange capacity and thermal stability in comparison with unpurified clay. These were then used in the synthesis of two thermally stable organoclays by replacing the interlayer sodium cations with two (alkyl and aryl) phosphonium surfactant cations to circumvent the problem of low temperature decomposition of quaternary ammonium organoclays usually used in polymer nanocomposites. The organoclay with aliphatic groups showed more compatibility with PA66 in comparison with the organoclay with aromatic groups. Thus, the use of organoclay with aliphatic groups resulted in nanocomposites with higher tensile strength, higher modulus, higher elongation at break, and higher impact strength in comparison with the nanocomposites produced from the organoclay with aromatic groups. © 2012 Wiley Periodicals, Inc. J. Appl. Polym. Sci. 000: 000–000, 2012

KEYWORDS: clay modification; organoclay; nanocomposite; phosphonium; thermal stability

Received 13 April 2011; accepted 23 March 2012; published online
DOI: 10.1002/app.37788

INTRODUCTION

Nanocomposites, specifically polymer–clay nanocomposites, constitute one of the most recent areas of research in nanotechnology. These materials can exhibit enhanced mechanical properties,[1–3] increased optical transparency,[4] improved gas barrier properties,[5] superior flame retardancy,[6,7] higher thermal stability,[8–11] and heat distortion temperature[12] at lower clay loadings compared with conventional polymer composites containing traditional fillers.

Layered silicates such as montmorillonite (MMT) which is a structural group of 2 : 1 phyllosilicates and an undergroup of smectites can be used for the synthesis of polymer–clay nanocomposites.[13] Pristine layered silicates usually contain hydrated sodium or potassium ions. Ion-exchange reactions with cationic surfactants, including primary, tertiary, and quaternary ammonium ions render the normally hydrophilic silicate surface organophilic, which makes intercalation of many engineering polymers possible and improves the wetting characteristics with the polymer[14–17] in which the surface energy of MMT decreases and the basal spacing expands.[18]

Organoclays are abundant, inexpensive, environment friendly, and above all essential to develop polymer nanocomposites. All of these properties attracted researchers to surface modification of clays to create new materials to be used in a wide spectrum of new applications.[19] The thermal stability and flammability performance of polymer nanocomposites is highly influenced by the processing stability of both the polymer and the organic-treated layered silicate. The low thermal stability of ammonium surfactants presents a problem for melt compounding and injection molding of polymer nanocomposites into final molded products. Such problems are commonly encountered at high processing temperatures exceeding 200°C: for example, in the melt processing of polyamides (PA6 and PA66), poly(ethylene terephthalate), and polycarbonate (PC). Thermal degradation during processing can initiate/catalyze polymer degradation, in addition to a variety of undesirable effects during processing and in the final product.[20,21] Phosphonium salts are capable of undergoing a wider range of reactions and behave differently than their ammonium counterparts because of the greater steric tolerance of the phosphorus atom in phosphonium salts and the participation of its low-lying d-orbitals in the processes of making and breaking chemical bonds.[8]

Additional Supporting Information may be found in the online version of this article.

Surface energy, basal spacing, and thermal stability of these organoclays depend strongly on the chemical structure, packing density, the degree of cation exchange, and the type of cation existing in the surfactant. Efforts have been made to synthesize thermally stable organoclays based on stibonium, phosphonium, or imidazolium surfactants. The phosphonium surfactants incorporate mainly short alkyl chains, benzene, and usually a long alkyl chain. These organoclays exhibit substantially higher thermal stability than ammonium surfactant modified organoclays. Additionally, phosphonium compounds enhance flame retardancy.[8,22]

The quantity of smectites (the major minerals of bentonite clays) is crucial to improve the quality of bentonites and affect their characteristics.[23] The presence of common impurities in bentonite clays, such as quartz, calcite, feldspar, mica, and organic matter,[24] negatively affect the cation exchange capacity (CEC) and thermal stability of bentonites.[25] Furthermore, purity is critical for reproducibly achieving maximum mechanical properties, less degradation of thermoplastics during the melt processing stages, and optimum clarity in packaging applications. Thus, the isolation of some smectite group minerals from bentonites by purification (sedimentation) is of great importance before the surface modification step.[23]

A wide variety of polymers, including thermoplastics, such as styrenics, polyolefins, etc., and thermosetting materials, such as epoxy resins and phenolics have been used as the starting materials in the production of nanocomposites.[26] Polyamide (PA66) is an important synthetic resin and is widely used in engineering plastics and fiber industries because of its excellent physical and mechanical properties. It is a flammable thermoplastic, and thus, anti-flaming modification is necessary in many cases of usage.[27] In recent years, the increasing interest in polyamides resulted from their high melting points to extend the boundaries of this polymer type to satisfy more stringent high temperature automobile and electronic applications. Its high melting point (about 265°C) is a function of both the strong hydrogen bonding between the chains and its crystal structure. Despite the fact that PA66 has good thermal stability, it tends to degrade when held for long periods of time at high temperatures. The adipic acid segments can cyclize, leading to chain scission, the production of cyclopentanone and derivatives, and evolution of carbon dioxide and ammonia. Crosslinking occurs and the material turns into an intractable gel along with reduction of molecular weight.[28]

Recent PA66 clay nanocomposites studies involved the preparation of nanocomposites with ammonium treated MMTs. Yu et al.[29] prepared Nylon-66 nanocomposites by melt-compounding nylon-66 with an alkyl ammonium surfactant pretreated MMT. The decomposition of the surfactant on the MMT occurred from 200°C to 500°C. It was proposed that MMT with more thermally stable surfactants has to be produced to increase the onset decomposition temperature of alkyl ammonium pretreated MMT when polymers with high melt-compounding temperatures are used.

This study is carried out to investigate the effects of purified and organically modified layered silicates on the morphology, melt flow properties, mechanical properties, and especially the thermal stability of polymer nanocomposites. The clays were purified by sedimentation and then surface modified by ion exchange using two phosphonium ionic liquids. These salts were: tetraoctyl phosphonium bromide (TO-P Br) and benzyltriphenyl phosphonium chloride (BZLTP-P Cl). The clay used in this study (B) was obtained from Na^+-bentonite rock mined from Tokat/Resadiye in Turkey. Polyamide 66 (PA66) was used as the polymer matrix for the production of the nanocomposites. Melt intercalation technique was performed by using a co-rotating twin-screw extruder to produce the polymer nanocomposites. PA66 organoclay nanocomposites were prepared using the modified organoclays with and without the use of an elastomer, which also acted as an impact modifier.

EXPERIMENTAL

Materials

The sodium MMT rich bentonite clay (KAR-BEN) used in this study was mined from Resadiye (Tokat/Turkey) and supplied by Karakaya Bentonit (Turkey). The raw bentonite clay (B) with elemental composition of $[Al_{1.47}Fe_{0.29}Mg_{0.23}][Al_{0.076}Si_{3.29}]O_{10}(OH)_2$ contained 90% MMT as reported by the supplier. The CEC of this bentonite was 67.5 meq/100 g clay, as determined by the methylene blue procedure. Phosphonium clay modifiers were purchased from Aldrich Company. Phosphonium surfactants with different chain groups (aryl and alkyl) attached to the phosphonium cation were used in the modification of the purified bentonites (PBs).

PA66 with trade name of Bergamid A65 was purchased from PolyOne Company, Istanbul-Turkey. Lotader® 2210 resin [a random terpolymer of ethylene (E), butyl acrylate (BA), and maleic anhydride (MAH)] was purchased from Arkema, France and used as an impact modifier for PA66. This elastomer contains anhydride groups, which can react with the amine ends of PA66.

Preparation of Organoclays

Raw bentonite clay was purified before organic surface modification to obtain highly pure clays by removing nonclay and other clay minerals. The steps of the purification procedure used were as follows.

A total of 50 g of dried Na-MMT clay sample (80°C for 12–15 h) and a small quantity of sodium pyrophosphate (to avoid agglomeration of bentonite-water mixture) were put into a 5 L flask. Distilled water was added into the flask in small portions while mixing with a stirrer and the temperature of the mixture was kept at 40°C for 2 h. After filling the flask with distilled water, the suspension stayed for 9 h for sedimentation. The upper 25 cm of the solution was siphoned and centrifuged at 6000 rpm for 10 min. The clay minerals collected at the end of centrifugation (~ 25 wt % of the starting amount) were dried in an oven at 120°C for 12 h.

To prepare phosphonium-treated PBs, the PBs were initially dried in vacuum at 120°C for 12 h. The amounts of the surfactants added to all clays were 1.1 times the CEC. Purified clay (10 g) was put into 1 L of distilled water at room temperature in a glass beaker equipped with a mechanical stirring bar. After 24 h, mixing was stopped and the system was heated until it reached 80°C. A solution of ethyl alcohol (400 mL) containing

the surfactant, at 1.1 times the CEC, was poured into the clay dispersion. Mixing was continued for 2 h at 80°C, and then, the organoclay was filtered and washed with hot water (80°C) using coarse Whatman filter paper. Washing was repeated at least three times until no halide traces were detected with silver nitrate. After washing, the organoclay was dried overnight at room temperature, followed by drying at 120°C for 24 h under vacuum. It was then ground in a mortar (<106 μm) and dried again under the same conditions and stored in a dessicator. Tetraoctyl phosphonium organoclays were greasy due to the insolubility of the salt itself, and thus, they could not be sieved to sizes less than 150 μm.

Preparation of Nanocomposites

PA66-based nanocomposites were prepared in air atmosphere by melt compounding using a co-rotating, intermeshing Thermoprism TSE 16 TC twin screw extruder with an L/D ratio of 24 (L = 384 mm, D = 16 mm). In addition to ternary PA66/organoclay/elastomer nanocomposites, PA66/organoclay binary nanocomposites and PA66/elastomer blend were also prepared for comparison purposes. Based on earlier investigations[13] as well as the current study, the optimum amounts of organoclay and elastomeric phase to balance the stiffness and toughness of the products were found to be 2 and 5 wt %, respectively. During the experiments, the feed rate, screw speed, and the temperature profiles were kept constant for PA66 at 25 g/min, 200 rpm and 260–275–275–275–280°C from the main hopper to the die, respectively.

Extrusion parameters are crucial to obtain good intercalation. PA66 nanocomposites and blends were extruded twice to increase the effect of shear intensity on the organoclay dispersion. After the first extrusion step, the extrudate was cooled in a cooling bath and pelletized using a chopper. The pellets of PA66 containing compounds obtained at the end of the process were stored in polyethylene bags and were all dried at 100°C under vacuum for 12 h before the next extrusion step or injection molding. Drying was performed in vacuum for 24 h at 120°C for the organoclays and for 12 h at 40°C for the elastomers, because elimination of physiabsorbed water is required before processing, to obtain materials with improved properties. Drying was repeated before each processing step, because the presence of even small traces of moisture can cause significant hydrolytic degradation of the materials.

The specimens were injection molded by a DSM Xplore laboratory scale micro injection molding machine. All the samples were injection molded immediately using the extrudate in the melt form. In this procedure, the injection mold barrel was attached to the extruder die. It was filled up with the melt and directly put into the ram type injection molding machine, and the samples were molded at a pressure of 15 bars. During the molding process, the injection barrel temperature was adjusted to 275°C, and the mold temperature was set to 60°C. All injected molded samples were kept for 24 h under vacuum in a dessicator before analysis.

Characterization Experiments

X-Ray Diffraction Analysis (XRD). RIGAKU D/MAX 2200/PC X-Ray diffractometer that generates a voltage of 40 kV and current 40 mA from monochromatic Cu Kα radiation source (λ = 1.5418) was used to analyze the organoclays and nanocomposites. The diffraction angle 2θ was scanned from 1° to 8° for the polymers (on dog bone-shaped tensile bars) and from 1° to 40° for clays/organoclays powders at a scanning rate of 2° per minute and a step size of 0.02°. To calculate the distance between the silicate layers, Bragg's law was used.

Transmission Electron Microscopy. For transmission electron microscopy (TEM) analysis, ultra sections of 70 nm in thickness were cryogenically cut with a diamond knife at a temperature of −100°C for polymer/organoclay binary and polymer/organoclay/elastomer ternary nanocomposites. All samples were trimmed parallel to the molding direction. These samples were examined by a Tecnai™ G2 F30 transmission electron microscope at an acceleration rate of 120 kV.

Scanning Electron Microscopy. To examine the failure mechanism and elastomer dispersion, the impact-fracture surface of the nanocomposites were scanned by a low voltage scanning electron microscope (JEOL JSM-6400). Nanocomposites containing elastomers were etched with boiling xylene for 6 h to extract the elastomeric phase. Scanning electron microscopy (SEM) photographs of the impact-fractured surfaces were taken at 4000× magnifications.

Melt Flow Index. Melt flow index (MFI) measurements were carried out using an Omega Melt Flow Indexer. Because MFI values are inversely related to the melt viscosity, changes in viscosity values were evaluated for each formulation. Conditions of temperature and load were selected as 275°C and 0.325 kg for PA66 (ISO 1333), which are in accordance with the material specifications.

Tensile Tests. Tensile tests were performed by using Shimadzu Universal Testing Machine AG-IS (100 kN) according to ISO 527. Tensile strength (MPa), Young's modulus (GPa), and percent elongation at break (%) were determined from the stress–strain curves. The strain rate was 0.1 min^{-1} and the test temperature was 23°C ± 2°C for all the samples.

Impact Tests. Charpy impact strength of notched specimens with the dimensions of 80 × 10 × 4 mm^3 was measured by pendulum Ceast Resil Impactor according to ISO 179. The tests were performed at 23°C ± 2°C, and the average of five test results was reported.

Thermal Gravimetric Analysis. Thermal gravimetric analysis (TGA) analysis was performed by a Shimadzu DTG-60H thermal analyzer under ultrahigh purity nitrogen atmosphere. The scanning rate used was 15°C/min for the clays, organoclays, and nanocomposites.

Differential Scanning Calorimetry. Differential scanning calorimetry (DSC) measurements were carried out under nitrogen atmosphere by using DSC-60 Shimadzu differential scanning calorimeter, to evaluate the possible changes in melting temperature (T_m) and percent crystallinity for each composition. Samples (~ 6.5 mg) were cut from dry tensile bars and were placed in the DSC aluminum pans. They were heated from 25 to 300°C at a heating rate of 10°C/min. Percent crystallinity was

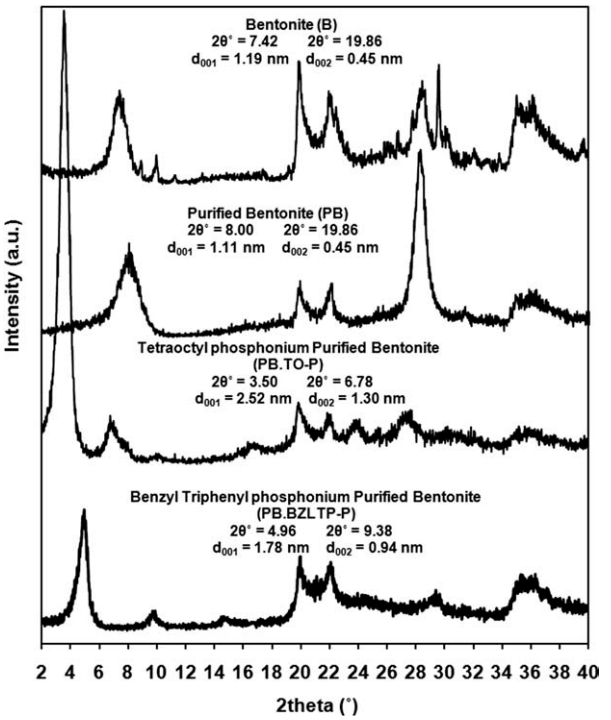

Figure 1. XRD patterns of bentonite (B), purified bentonite (PB) unmodified and modified by TO-P Br salt (PB.TO-P) and BZLTP-P Cl salt (PB.BZLTP-P).

calculated by using the heat of fusion of the specimen. The heat of fusion for 100% crystalline PA66 was taken as 206 J/g.[2]

RESULTS AND DISCUSSION

XRD Analysis

The XRD diffraction patterns of the clays, raw bentonite (B), PB, and PB modified with tetraoctyl phosphonium bromide (PB.TO-P) and benzyltriphenyl phosphonium chloride (PB.BZLTP-P) used in this study were obtained. XRD patterns of the clays and organoclays are shown in Figure 1.

The XRD results of this investigation showed that the clay deposits from Resadiye mainly consisted of MMT with some amounts of impurities. The raw bentonite clay (B) contained nonclay minerals such as analcime, calcite, clinoptilolite, dolomite, feldspar, quartz, illite, opal-C, and α-cristobalite. The PB, however, did not contain most of these impurities, except for negligible amounts of quartz and α-cristobalite. In addition, the purification process increased the CEC of the bentonite clays from 67.5 meq/100 g clay to 95 meq/100 g clay.[25] The interlayer distance of bentonite decreased slightly after purification from 1.19 nm to 1.11 nm. This change can be attributed to the elimination of a portion of the monomolecular water layer between the MMT layers.[20]

The values of basal spacing determined for pristine purified clay PB increased, upon intercalating the TO-P Br and BZLTP-P Cl salts inside the layers, from 1.11 nm up to 2.52 nm and 1.78 nm, respectively. The low molecular weight surfactant (BZLTP-P Cl with the phenyl and benzyl groups) led to a smaller basal spacing (1.78 nm) corresponding to a bilayer arrangement of chains. High molecular weight surfactants (TO-P Br with long alkyl chains) produced organoclays with a higher basal spacing (2.52 nm) indicating an arrangement between pseudo-trilayers and paraffin-type of alkyl chains.[22,30,31]

The initial basal spacing in the organoclay is an important parameter for the determination of the potential for polymer intercalation and clay mineral delamination. Organoclays with smaller interlayer distances have reduced probabilities for polymer intercalation. Nevertheless, intercalated structures can also be prepared from clay minerals with small basal spacing via *in situ* polymerization.[20] In general, it is desirable to start with organoclays that exhibit large interlayer distances, to achieve desirable nanocomposites properties.[22] However, if the salt is too big, then the polymer chains cannot diffuse into the interlayer spacing.

XRD patterns for (PB.TO-P) organoclay and the nanocomposites produced (PA66/PB.TO-P) and (PA66/PB.TO-P/E-BA-MAH) are shown in Figure 2(a).The d-spacing of these materials are 2.58 nm, 2.00 nm, and 2.00 nm, respectively. The reduction in the d-spacing after heating and cooling of organic-modified bentonite has been attributed to recrystallization of the polymeric matrix, which occurs during cooling after extrusion[20] or high temperature oxidative degradation. Another explanation is the evaporation of the organic phase while drying of the organoclay. A third possible argument is the high pressure, which causes the

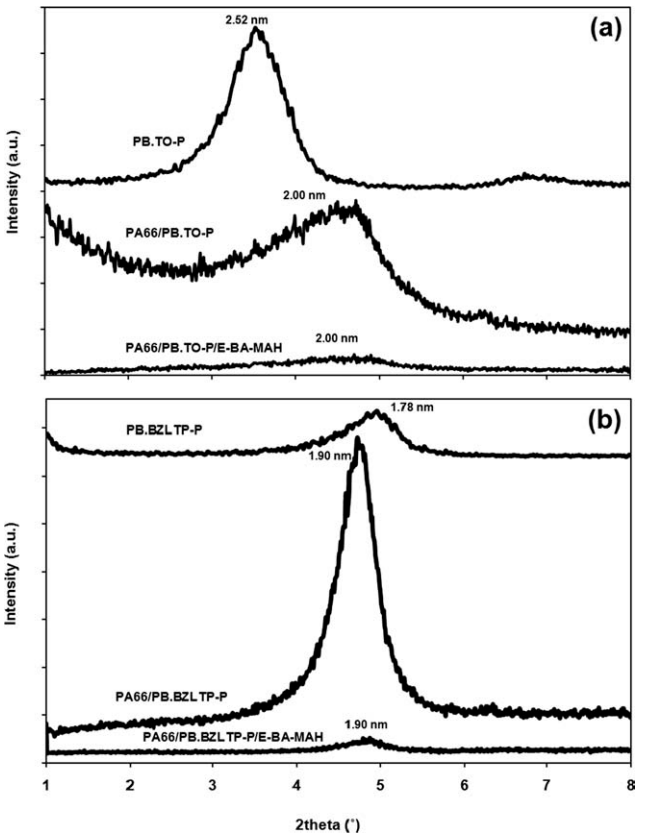

Figure 2. XRD patterns of (a) PB.TO-P, PA66/PB.TO-P and PA66/PB.TO-P/E-BA-MAH and (b) PB.BZLTP-P, PA66/PB.BZLTP-P, and PA66/PB.BZLTP-P/E-BA-MAH.

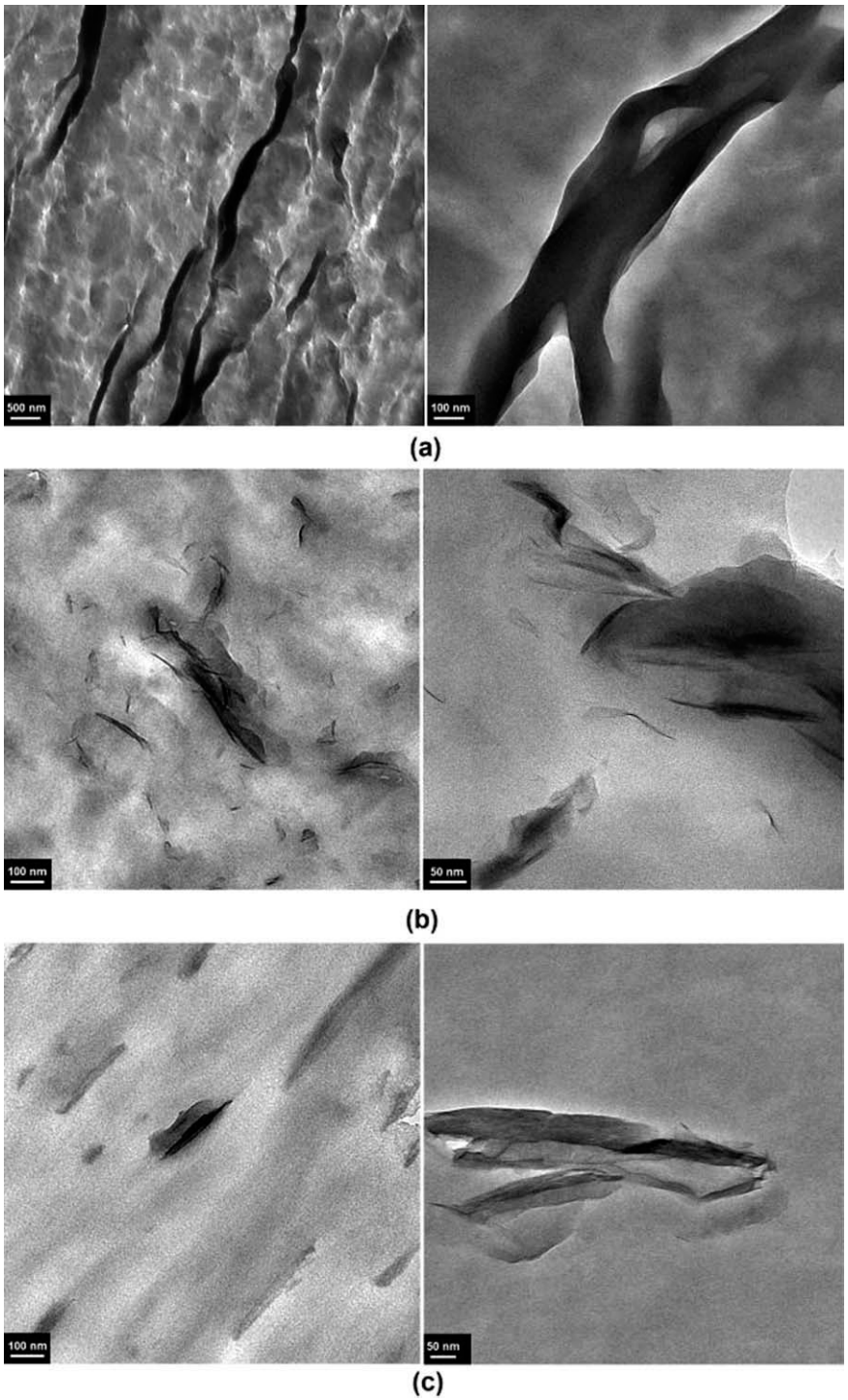

Figure 3. TEM micrographs of (a) PA66/E-BA-MAH blend: (i) 500 nm, (ii) 100 nm, (b) PA66/PB.TO-P/E-BA-MAH ternary nanocomposite: (i) 100 nm and (ii) 50 nm, and (c) PA66/PB.BZLTP-P/E-BA-MAH ternary nanocomposite: (i) 100 nm and (ii) 50 nm.

clay layers to collapse during injection molding. It is likely that one or a combination of these mechanisms took place.

XRD patterns for (PB.BZLTP-P) organoclay and the PA66 binary and ternary nanocomposites with PB.BZLTP-P and E-BA-MAH are presented in Figure 2(b). The X-ray diffraction patterns of these nanocomposites revealed a slight increase in the basal distance of these planes from 1.78 nm to 1.90 nm. Thus, for (PB.BZLTP-P) organoclay, the X-ray patterns indicate a slightly intercalated structure upon compounding with the polymer.

TEM Analysis

Figure 3(a–c) displays the TEM images of PA66/E-BA-MAH blend and PA66-phosphonium ternary nanocomposites (PA66/PB.TO-P/E-BA-MAH and PA66/PB.BZLTP-P/E-BA-MAH) at

different magnifications. In Figure 3(a), the bright areas shown at both small and large magnifications indicate the polymer matrix and the elastomeric phase is indicated by the darker area. The PA66/E-BA-MAH interphase is clear through the sharp line between the PA66 and elastomer phases.

In ternary nanocomposites, the black spots represent the clay agglomerates in TEM micrographs. The dark lines shown at high magnifications are the transverse sections of single or possibly multiple silicate platelets.[32] For well-dispersed structures, these spots appear as ribbons that indicate the delaminated layers of the filler. The incorporation of the organoclays in polymer/elastomer/organoclay ternary nanocomposites is expected to reduce the interfacial tension between the polymer and elastomer. The organoclay addition reduced the interfacial tension and led to a decreased elastomeric domain size. This reduction is clearly seen in Figure 3(b,c). In this case, the organoclay particles are localized inside the elastomeric phase and at the interphase between the PA66 and E-BA-MAH. TEM micrographs show that PB.TO-P containing PA66 ternary nanocomposite exhibit higher d-spacing than PB.BZLTP-P containing PA66 ternary nanocomposite. Furthermore, it is clear that PB.TO-P layers are intercalated and dispersed, whereas PB.BZLTP-P exhibits more agglomerates rather than dispersed structure. This can be attributed to the higher initial basal spacing of the organoclay PB.TO-P (2.52 nm) in comparison with the smaller initial basal spacing of PB.BZLTP-P (1.78 nm). Upon melt compounding, the basal spacing of PB.TO-P decreases to 2.00 nm, whereas the basal spacing of PB.BZLTP-P increases to 1.90 nm. Thus, in the polymer matrix, PB.TO-P still has a higher d-spacing than PB.BZLTP-P does.

SEM Analysis

The SEM micrographs of the PA66 compositions are shown in Figure 4. Extensive ductile shearing is evident on the fracture surface of the unfilled PA66 system, indicating the well-known shear mechanisms of PA66. The bulk polymer is drawn and broken under tension in the crack propagation direction.

The addition of E-BA-MAH compatibilizer to the unfilled PA66 system increased the tortuousity and shortened the crack propagation lines [Figure 4(b)]. The average domain sizes calculated for the samples are given in Table I. The addition of E-BA-MAH is known to form a graft copolymer during the blending process by the imidation reactions. This graft copolymer either forms at or migrates to the interface between the polymer and elastomer, lowering the interfacial energy, and improving the interfacial adhesion. In this manner, it contributes to the stability of the dispersed phase against segregation during further processing. The imidation reaction changes the chemical nature of the interface, which in turn reduces the interfacial tension and retards particle coalescence.[15] In addition, the compatibilizer used functions as an impact modifier which compensates for the decrease in toughness caused by the incorporation of the organoclay into the polymer matrix. This effect is clearly seen in the mechanical properties because the toughness of PA66 increased from 7.0 to 10.4 kJ/m^2 upon blending with only 5 wt % of E-BA-MAH.

PA66/organoclay binary and PA66/organoclay/E-BA-MAH ternary nanocomposites are shown in Figure 4(c–f). Although clay agglomeration can be observed in some of the nanocomposites that may facilitate mechanical failure, the mechanical properties of the nanocomposites exhibited significant improvement. The toughness of the materials is dependent on the average domain size and interdomain distance. Clay platelets may act as barriers to prevent coalescence of dispersed phase and thus cause reduction in domain sizes because of their high aspect ratio. The E-BA-MAH domains in the PB.TO-P ternary nanocomposites in this study (177.3 nm) were found to be smaller compared with the blend (182.0 nm). However, PB.BZLTP-P ternary nanocomposite (188.9 nm) showed the opposite effect. The presence of anhydride functional groups immobilized the interface and prevented the coalescence of elastomeric domains both in the nanocomposites and in the blend by forming chemical bonds with the PA66 matrix. The anhydride group is capable of reacting with the amine ends. PB.TO-P exhibited better compatibility with PA66, whereas PB.BZLTP-P exhibited lower toughness and mechanical properties, as shown later.

Melt Flow Analysis

MFI values of PA66 compositions are given in Table II. The melt viscosity of PA66 did not change significantly after extrusion twice, indicating negligible degradation during extrusion. E-BA-MAH has a much lower MFI (higher viscosity) than PP66 does. PA66/E-BA-MAH blend has an MFI (25.2 g/min) that is in between those of PA66 and E-BA-MAH. The anhydride group present in the elastomer E-BA-MAH with high melt viscosity (low MFI of 4.5 g/min) has the potential of reacting with the amine ends of PA66. Overall, the effect of E-BA-MAH on MFI was much higher than the effect of the organoclays. In addition, a systematic correlation could not be found regarding the structure of the organoclays, which exhibited close MFI values.

The addition of fillers into the polymer matrix may retard the flow especially at low shear rates and cause an increase in the melt viscosity (decrease in MFI). This is mainly dependent on the shape, size, and concentration of the filler. However, in this study, the melt viscosity decreased slightly (MFI increased) in PA66/phosphonium organoclay binary nanocomposites in comparison with PA66 (twice extruded). This behavior can be ascribed to the slip between the polymer matrix and the dispersed clay platelets.[13,33,34]

The melt flow behavior of nanocomposites depends on the degree of dispersion of organoclay aggregates (i.e., morphology). The later depends on many factors including the degree of compatibility between polymer matrix and organoclay. The viscosity of the polymer matrix is an important factor that affects the dispersion of organoclays. The intercalation and/or exfoliation requires the diffusion of polymer chains into the silicate layers or peeling away the top and bottom layers as promoted by the polymer adsorption and by the application of shear stress.[35] With increasing viscosity, the shear stress applied to the platelets increases and leads to the separation of clay layers. Thus, the addition of organoclays to PA66/E-BA-MAH blend slightly decreased MFI (increased the viscosity) of the blend.

Mechanical Properties

The tensile properties of all PA66 compositions and E-BA-MAH are shown in Table III. The addition of E-BA-MAH elastomer

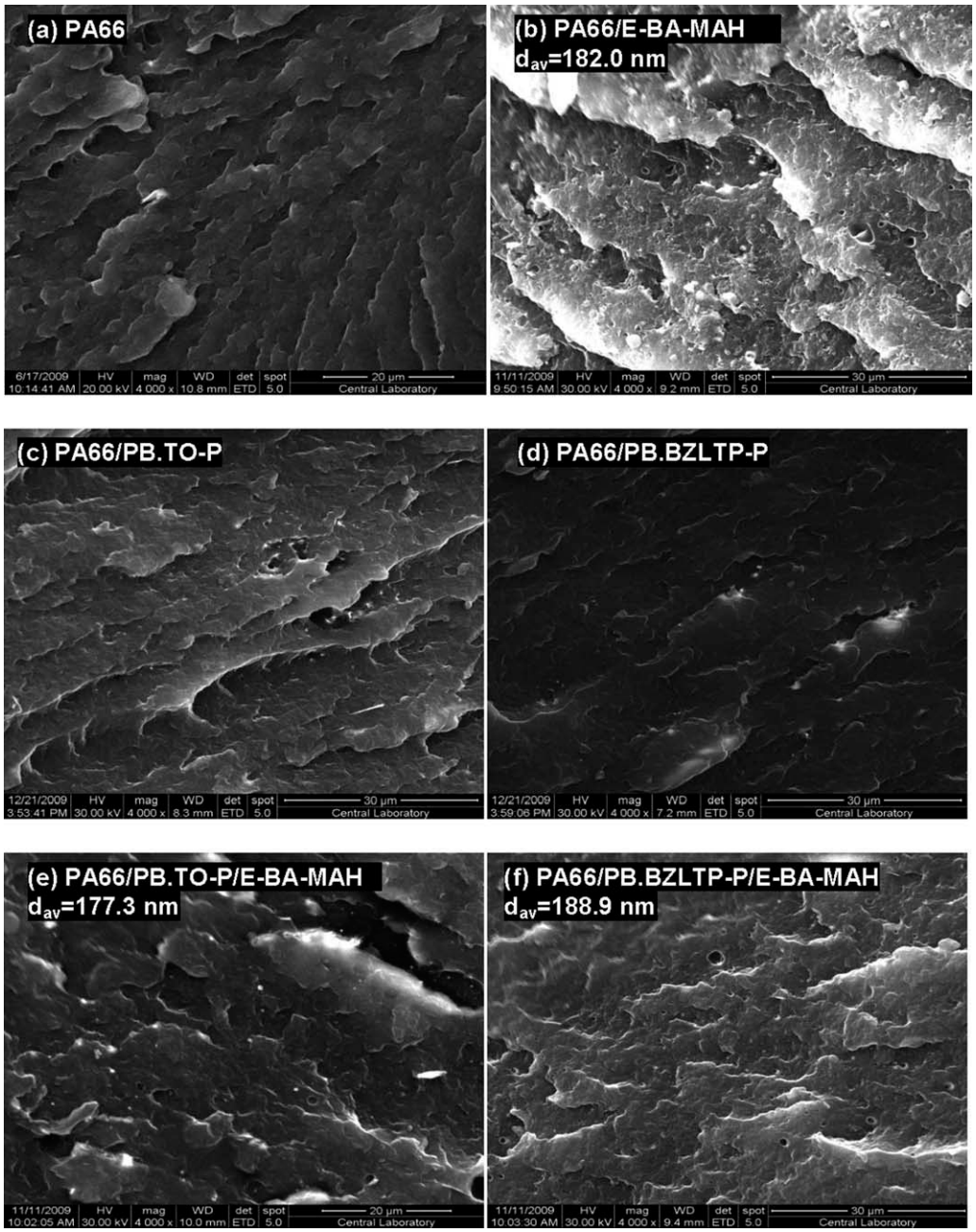

Figure 4. SEM micrographs of PA66-based compositions.

with low tensile strength and Young's modulus decreases the tensile strength and Young's modulus of PA66. In elastomer modified polymers, yielding or crazing occurs around the elastomeric domains and a higher amount of energy is absorbed by the polymer.[36] On the other hand, phosphonium organoclays stiffen the matrix in PA66/PB.TO-P and PA66/PB.BZLTP-P binary nanocomposites resulting in an increase in the tensile strength and Young's modulus. The high aspect ratio of the organoclay contributes to the reinforcement effect, because it creates a large contact area with the polymeric matrix. The interfacial adhesion between PA66 and the organoclay is also significant in dispersing the clay homogeneously in the polymer matrix and increasing the strength of the material. In the binary nanocomposites, this effect is observed better with PB.TO-P organoclays, which exhibit higher tensile strength and Young's modulus than PB.BZLTP-P does, because of the better dispersion of PB.TO-P. The compatibility of the organoclay with PA66 matrix and the elastomer, in addition to the initial basal spacing of the organoclay PB.BZLTP-P (1.78 nm) which is smaller than the initial basal spacing of PB.TO-P (2.52 nm), are crucial factors to the mechanical properties of the nanocomposite. These results are consistent with TEM analyses which showed that PB.TO-P layers are intercalated and dispersed in the elastomeric phase, whereas PB.BZLTP-P exhibited more agglomerates rather than dispersed structure.

Table I. Average Domain Sizes of PP66-Based Samples

Composition	d_{av}[a] (nm)
PA66 (not extruded)	–
PA66 (extruded twice)	–
PA66/E-BA-MAH	182.0
PA66/PB.TO-P/E-BA-MAH	177.3
PA66/PB.BZLTP-P/E-BA-MAH	188.9

[a]Average domain size.

PA66/phosphonium organoclay/E-BA-MAH ternary nanocomposites exhibited the expected decrease in strength and modulus as a result of the elastomer addition. This decrease was substituted by organoclays addition. The compatibility of PB.BZLTP-P/PA66 is also weaker compared with PB.TO-P/PA66 after the addition of E-BA-MAH elastomer.

E-BA-MAH caused ~ 9% increase in the elongation at break of the PA66 blend. The high elongation at break value of PA66, however, was diminished upon addition of organoclay in PA66 binary and ternary nanocomposites, because the inorganic silicate particles cannot be strained by external stresses. Upon addition of the organoclay, the spherulite size also decreases in PA66 leading to brittle structure clearly seen in PA66/phosphonium organoclay binary nanocomposites. The decrease in the elongation at break is balanced by the addition of the elastomer E-BA-MAH in the phosphonium organoclay ternary nanocomposites. The elongation at break, tensile strength, and Young's modulus were better in the case of PB.TO-P-based ternary nanocomposite compared with PB.BZLTP-P-based ternary nanocomposite.

Impact strengths of PA66, PA66 blend, and PA66 nanocomposites are shown in Table III. Impact strength of PA66/E-BA-MAH blend increased from 7.0 kJ/m^2 for pure PA66 to 10.4 kJ/m^2 because of the cavitation mechanism introduced by the elastomer. The impact strength of PA66/organoclay binary nanocomposites decreased slightly using PB.BZLTP-P, whereas it remained constant upon using PB.TO-P organoclay. Among the PA66 ternary nanocomposites, PB.TO-P exhibited an impact strength value of 9.0 kJ/m^2 which is higher than that of PB.BZLTP-P which exhibited a lower value (7.8 kJ/m^2).

The organoclay dispersion is better in PB.TO-P containing PA66 binary and ternary nanocomposites in comparison with the PB.BZLTP-P binary and ternary nanocomposites, and this is clearly reflected in the toughness of the nanocomposites. This observation is also consistent with the TEM and SEM analyses discussed earlier. Although in the ternary nanocomposites exfoliation of the organoclays was not totally achieved, some of the clay agglomerates were broken down and the polymer chains could penetrate between the clay platelets. Thus, the toughness of the PA66 ternary nanocomposites was improved with respect to the binary nanocomposites.

Table II. MFI Results of PA66-Based Compositions

Composition	MFI (g/10 min)
PA66 (not extruded)	36.5 ± 1.9
PA66 (extruded twice)	36.0 ± 1.7
E-BA-MAH	4.5 ± 0.3
PA66/E-BA-MAH	25.2 ± 1.2
PA66/PB.TO-P	37.1 ± 2.1
PA66/PB.BZLTP-P	38.0 ± 2.0
PA66/PB.TO-P/E-BA-MAH	24.5 ± 2.6
PA66/PB.BZLTP-P/E-BA-MAH	24.8 ± 1.0

Thermal Analysis

Thermogravimetric Analyses of Surfactants, Clays and Organoclays. The thermal gravimetric analyses of the surfactants, clays, phosphonium organoclays, and PA66 nanocomposites were performed to investigate the effects of salts used on the clay and the resulting nanocomposites. Thermogravimetric measurements (TG/DrTGA) were carried out under nitrogen atmosphere and the results are reported in Tables IV and V in terms of onset decomposition temperature and peak decomposition temperature from derivative thermograms.

The alkyl phosphonium salt exhibited a higher onset decomposition temperature of 360°C (2.3% mass loss) compared with the aryl phosphonium salt with an onset decomposition temperature of 340°C (0.1% mass loss). The thermal decomposition of TO-P Br and BZLTP-P Cl (temperature at 5% mass loss) started at 329°C and 339°C, respectively. On the other hand, the maximum decomposition rate from derivative TGA curves was 387°C for TO-P Br and 345°C for BZLTP-P Cl. At 200°C, both surfactants exhibited no mass loss, and at 275°C, only TO-P Br exhibited 0.66% mass loss. Thus, considering polymer processing temperatures in the range of 200–300°C, phosphonium surfactants exhibited superior thermal stability in comparison with the ammonium-based surfactants.

Table III. Mechanical Property Data of PA66-Based Compositions

Composition	Tensile strength (MPa)	Young's modulus (GPa)	Elongation at break (%)	Impact strength (kJ/m^2)
PA66 (extruded twice)	83.7 ± 3.7	2.73 ± 0.13	23.3 ± 0.2	7.0 ± 0.3
E-BA-MAH	12.0 ± 0.3	–	600.0 ± 9.0	–
PA66/E-BA-MAH	76.1 ± 1.7	2.43 ± 0.03	25.8 ± 1.1	10.4 ± 0.8
PA66/PB.TO-P	89.6 ± 0.9	2.94 ± 0.04	13.9 ± 0.5	7.0 ± 0.2
PA66/PB.BZLTP-P	88.8 ± 0.2	2.77 ± 0.03	12.2 ± 0.9	6.2 ± 0.1
PA66/PB.TO-P/E-BA-MAH	82.9 ± 0.7	2.54 ± 0.02	24.3 ± 0.8	9.0 ± 0.3
PA66/PB.BZLTP-P/E-BA-MAH	74.2 ± 1.0	2.35 ± 0.04	14.7 ± 2.0	7.8 ± 0.5

Table IV. Thermal Decomposition Results of Clays, Salts, and Organoclays

Material	T_{onset}[a] (°C)	Mass loss at T_{onset} (%)	Mass loss at 275°C (%)	Decomposition temperature at 2% mass loss (°C)	Decomposition temperature at 5% mass loss (°C)	$T_{max.\ D.R.}$[b] (°C)
Clay						
B	628	3.00	1.90	299	666	689
PB	653	2.42	1.31	533	769	728
Salt						
TO-P Br	360	2.3	0.66	302	329	387
BZLTP-P Cl	340	0.1	0.00	338	339	345
Organoclay						
PB.TO-P	327	0.88	1.45	290	338	513
PB.BZLTP-P	354	2.75	1.95	284	380	474

[a]T_{onset}: temperature corresponding to the cross section of the two tangents around the main degradation point in TGA thermogram., [b]$T_{max.\ D.R.}$: temperature at maximum decomposition rate.

The thermal stability of the clay itself as a starting material is crucial in the preparation of thermally stable organoclays. The impurities that exist in the raw bentonite negatively affect its thermal stability as well as the CEC. Figure 5 shows the TGA of the raw and PBs. All thermograms showed main decomposition temperatures in the range of 600°C and 700°C. After purification, the thermal stability of the bentonite clay increased significantly (~ 5% less weight loss) because of the release of inorganic minerals that cause thermal instability of the clay. The onset decomposition temperatures for B and PB were 628°C (3.0% mass loss) and 653°C (2.42% mass loss), respectively. In addition, the maximum decomposition rate from derivative TGA curves was 689°C for B and 728°C for PB. The thermal decomposition of B and PB (temperature at 5% mass loss) began at 666°C and 769°C, respectively. These results confirm the importance of purification of the raw bentonites before the ion exchange process.

Thermal decomposition of ammonium salts generally follows either a Hoffmann elimination reaction or an SN2 nucleophilic substitution. Phosphonium-modified MMT decompose at higher temperatures than ammonium organoclays, although phosphonium surfactants are susceptible to similar reactions. Hoffmann elimination occurs in the presence of basic anions, such as hydroxyl groups, which extract hydrogen from the alkyl chain of the quaternary ammonium, yielding an olefinic and tertiary amino group.[8] The nonisothermal decomposition of quaternary phosphonium modified MMT (PB.TO-P and PB.BZLTP-P) given in Figure 6(a,b) can be briefly revealed in the regions mentioned earlier. Below 180°C, the evolution of absorbed water and gaseous species, such as physiabsorbed CO_2 and N_2, occurs. Between 250°C and 500°C, organic substances evolve. Dehydroxylation of the aluminosilicate occurs from 500°C to 700°C and evolution of products associated with residual organic carbonaceous residue occurs between 700°C and 1000°C.[8] The region of interest for the production of polymer/organoclay nanocomposites exist below 500°C. In this region, the release of small molecules associated with fabrication and storage of the phosphonium organoclay or the evolution of decomposition products may modify interfacial energies between the silicate and polymer.

The chemical structure of the salts controlled the thermal stability of the organoclays in which the phenyl and benzyl substituted organoclay PB.BZLTP-P exhibited better thermal stability (Table IV). The aryl group substituted phosphonium organoclay (PB.BZLTP-P) showed a higher thermal stability of 380°C (5% decomposition) compared with 338°C for the alkyl substituted phosphonium organoclay (PB.TO-P). Similar results were obtained for the onset temperature of the organoclays. On the other hand, the maximum decomposition rate from derivative

Table V. Thermal Decomposition Results of PA66-Based Compositions

Composition	T_{onset}[a] (°C)	Decomposition temperature at 2% mass loss (°C)	Decomposition temperature at 5% mass loss (°C)	Mass loss at 275°C (%)	Char yield at 600°C (%)
PA66	408	365	392	1.20	4.1
PA66/E-BA-MAH	403	370	392	0.89	2.4
PA66/PB.TO-P	432	378	408	0.34	9.0
PA66/PB.BZLTP-P	427	381	410	0.59	3.5
PA66/PB.TO-P/E-BA-MAH	415	380	400	0.66	3.0
PA66/PB.BZLTP-P/E-BA-MAH	412	368	397	1.16	3.1

[a]T_{onset}: Temperature corresponding to the cross section of the two tangents around the main degradation point in TGA thermogram.

Applied Polymer SCIENCE

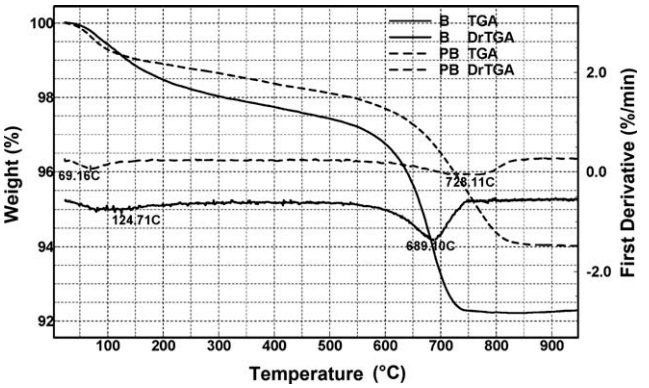

Figure 5. TGA thermograms of bentonite (B) and purified bentonite (PB).

TGA curves was 513°C for PB.TO-P and 474°C for PB.BZLTP-P. At 275°C, the mass loss of alkyl PB.TO-P and aryl PB.BZLTP-P organoclays was 1.45% and 1.95%, respectively. These results are in consistent with the alkyl and/or aryl phosphonium organoclays study done by Patel et al.[11] In addition, these temperature values are relatively higher than the processing temperatures of PA66 matrix used in this study.

Thermogravimetric Analyses of PA66 Compositions. The thermal stability of the surfactant molecules used is crucial in the production of PA66 nanocomposites because of the high

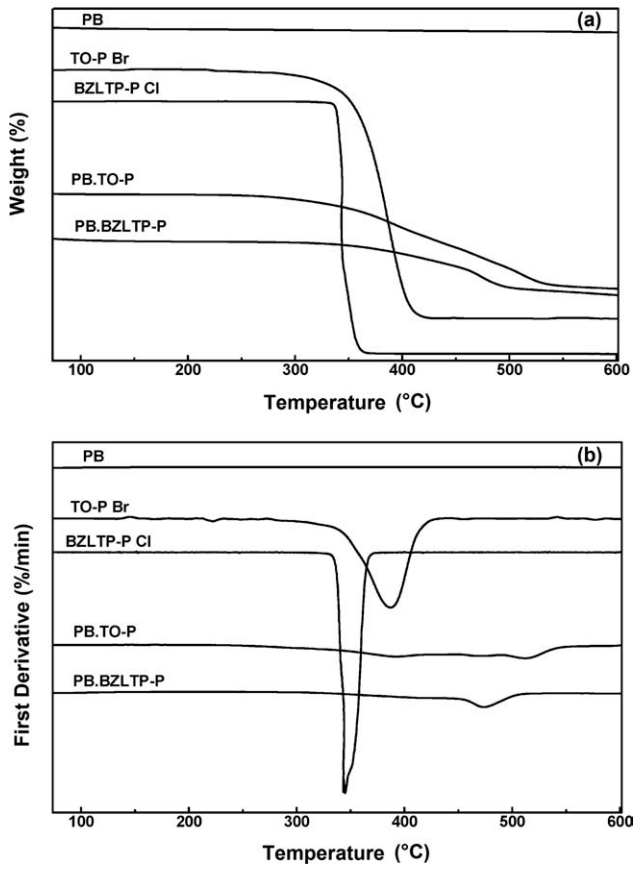

Figure 6. TGA thermograms of purified bentonite (PB), phosphonium salts, and modified organoclays.

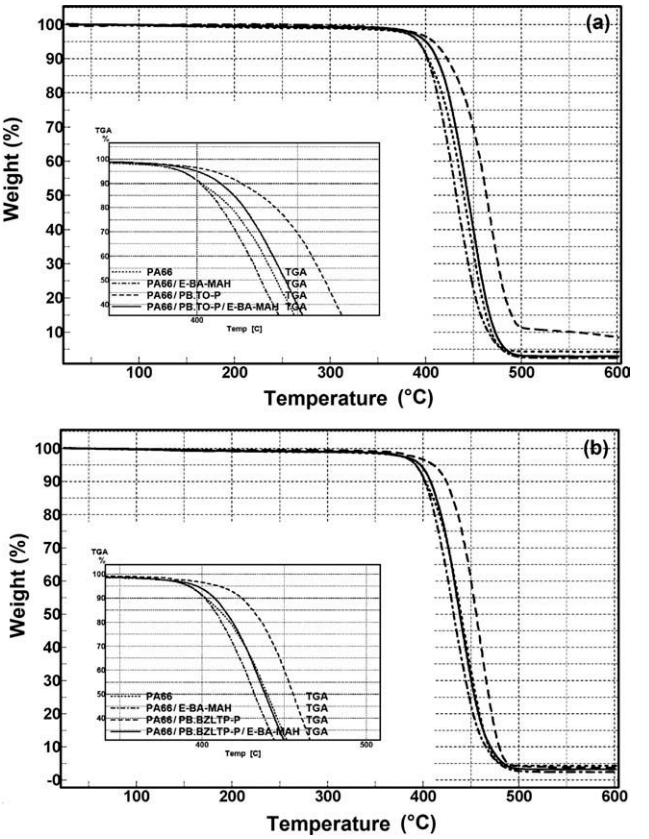

Figure 7. TGA thermograms of (a) PA66, PA66/E-BA-MAH, PA66/PB.TO-P, and PA66/PB.TO-P/E-BA-MAH and (b) PA66, PA66/E-BA-MAH, PA66/PB.BZLTP-P, and PA66/PB.BZLTP-P/E-BA-MAH.

melting temperature of PA66. The most commonly used quaternary ammonium surfactants are not sufficiently stable at temperatures above 200°C. It has been shown that the combination of high processing temperatures and high shear stresses causes even more degradation than high temperatures without shear.[37] For short processing times, the degradation is not problematic in the case of PA6 (processed at 240°C), whereas for PA66 melt processing temperatures (minimum 270°C) the problem is more serious. It has been reported that PA66 nanocomposites cannot be prepared via the same process with the same modified silicates, whereas other authors showed possible preparation with reasonably good results.[37]

The thermal decomposition data of all PA66 compositions taken under nitrogen atmosphere are given in Table V. Figure 7(a,b) presents the TGA graphs of PB.TO-P and PB.BZLTP-P containing nanocomposites compared with pure PA66 and the PA66/E-BA-MAH blend. It is clear that the addition of the E-BA-MAH elastomer into PA66 results in earlier decomposition of the PA66/E-BA-MAH blend in comparison with pure PA66. This decrease resulting from using the elastomer is compensated by higher mechanical properties and higher toughness of the blend. Qin et al.[27] studied the thermal stability and flammability of PA66/ammonium organoclay nanocomposites. When compared with the pristine polymer, the onset decomposition temperature of the binary nanocomposite was 10°C lower than that of pure PA66 in nitrogen atmosphere. The thermal behavior of the

Table VI. Thermal Properties of PA66-Based Compositions

Composition	T_m[a] (°C)	ΔH_f[b] (J/g)	Crystallinity (%)
PA66 (extruded twice)	264.9	53.4	25.9
PA66/E-BA-MAH	263.6	74.8	38.2
PA66/PB.TO-P	263.5	66.6	33.0
PA66/PB.BZLTP-P	265.9	66.6	33.0
PA66/PB.TO-P/ E-BA-MAH	265.5	61.7	32.2
PA66/PB.BZLTP-P/ E-BA-MAH	267.3	68.6	35.8

[a]T_m: melting temperature, [b]ΔH_f: heat of fusion.

nanocomposites in nitrogen atmosphere indicated that the addition of MMT accelerated the thermal decomposition of the PA66 matrix. This acceleration was attributed by the researchers to chain cleavage by water evolved from MMT (adsorbed or from dehydroxylation).[38] However, in this case, using thermally stable phosphonium organoclays revealed that the barrier effect of the silicate layers was dominant, because of the formation of carbonaceous-silicate char on the surface of nanocomposite. Thus, the onset decomposition temperature was 24°C and 19°C higher in PA66/PB.TO-P and PA66/PB.BZLTP-P binary nanocomposites, respectively, in comparison with PA66. The onset decomposition temperature for PA66/PB.TO-P and PA66/PB.BZLTP-P binary nanocomposites was 432°C and 427°C, respectively. On the other hand, PA66/phosphonium organoclay/E-BA-MAH ternary nanocomposites exhibited improvement in thermal stability compared with the pristine PA66 polymer and a decrease in the onset decomposition temperature compared with PA66 binary nanocomposites because of the presence of the elastomer. The onset decomposition temperature of PA66/PB.TO-P/E-BA-MAH and PA66/PB.BZLTP-P/E-BA-MAH ternary nanocomposites was 415°C and 412°C, respectively.

Differential Scanning Calorimetry Results of PA66 Nanocomposites

DSC thermograms of pure PA66, PA66/E-BA-MAH blend, and binary and ternary nanocomposites were obtained (Supporting Information Figures S1–S6). Crystallinity of the polyamide phase in all the combinations was determined by DSC analysis, and the results are given in Table VI.

The melting temperature of PA66 did not significantly change upon blending with E-BA-MAH. However, the crystallinity increased significantly in the presence of E-BA-MAH, because of enhanced nucleation.

The degree of crystallinity was found to be dependent on additives such as the organoclay and the elastomer in PA66 nanocomposites. Also, the melting point did not significantly change in PA66/phosphonium organoclay binary nanocomposites. Because of heterogeneous nucleation by organoclays, the crystallinity of PA66 increased by 7% upon adding the phosphonium organoclays (33.0%) compared with 25.9% for pure PA66. The crystallization of PA66/organoclay nanocomposites proceeds mainly via heterogeneous nucleation due to the large number of clay layers, whereas the crystallization of the neat PA66 precedes via both heterogeneous and homogeneous nucleation mechanisms. Homogeneous nucleation requires a low temperature to form stable nucleation, because it starts spontaneously by chain aggregation below the melting point. On the other hand, heterogeneous nuclei form simultaneously as soon as the sample reaches the crystallization temperature. Thus, the temperature to reach the maximum crystallization rate in neat PA66 is expected to be lower than that of PA66/organoclay binary nanocomposites.[39]

In general, it has been shown that the clay layers affect the formation of the lamellae, spherulites, crystallization rate, and also the crystalline phase. It was proposed by several investigators that an increase in crystallinity or spherulite size in polymeric materials can increase tensile strength and Young's modulus and decrease impact strength and elongation at break. These effects are clearly seen in the mechanical properties of PA66 binary nanocomposites, in addition to the mechanical effects of the organoclay. The tensile strength and Young's modulus of binary nanocomposites PA66/PB.TO-P (89.6 MPa and 2.94 GPa) and PA66/PB.BZLTP-P (88.8 MPa and 2.77 GPa) increased compared with pure PA66 (83.7 MPa and 2.73 GPa). The elongation at break and impact strength values of PA66/PB.TO-P (13.9% and 7.0 kJ/m^2) and PA66/PB.BZLTP-P (12.2% and 6.2 kJ/m^2) decreased in general compared with pure PA66 (23.3%, 7.0 kJ/m^2).

The tensile strength and Young's modulus of the ternary nanocomposites PA66/PB.TO-P/E-BA-MAH (82.9 MPa and 2.54 GPa) and PA66/PB.BZLTP-P/E-BA-MAH (74.2 MPa and 2.35 GPa) decreased compared with pure PA66 and the binary nanocomposites due to the presence of the elastomeric phase. The elongation at break values of the ternary nanocomposites PA66/PB.TO-P/E-BA-MAH (24.3%) and PA66/PB.BZLTP-P/E-BA-MAH (14.7%) increased compared with the corresponding the binary nanocomposites. PB.TO-P containing ternary nanocomposite exhibited impact strength of 9.0 kJ/m^2 and a crystallinity of 32.2%. On the other hand, PA66/PB.BZLTP-P/E-BA-MAH ternary nanocomposite with the highest crystallinity (35.8%) exhibited a lower impact strength of 7.8 kJ/m^2.

CONCLUSIONS

The purification of bentonites by sedimentation isolates the smectite portion and produces highly pure MMT with improved properties such as high CEC and high thermal stability. The surface modification of the pure MMT with suitable phosphonium surfactants resulted in thermally stable organoclays, which overcame the thermal degradation problem of conventional organoclays produced by alkyl ammonium surfactants when used with high melting-point polymers such as PA66 during compounding and processing. Their use can also result in better mechanical properties. The organoclay PB.TO-P with aliphatic groups showed higher compatibility with PA66 compared with PB.BZLTP-P with aromatic groups. Thus, the use of PB.TO-P resulted in nanocomposites with higher tensile strength, higher modulus, higher elongation at break, and higher impact strength compared with the nanocomposites produced from PB.BZLTP-P.

ACKNOWLEDGMENTS

The authors thank Karakaya Bentonit A.S., Ankara, Turkey for providing the raw bentonite.

REFERENCES

1. Shen, L.; Phang, I. Y.; Chen, L.; Liu, T.; Zeng, K. *Polymer* **2004,** *45*, 3341.
2. Yu, Z. Z.; Yan, C.; Yang, M.; Mai, Y. W. *Polym. Int.* **2004,** *53*, 1093.
3. Yilmazer, U.; Ozden, G. *Polym. Compos.* **2006,** *27*, 249.
4. Alexandre, M.; Dubois, P. *Mater. Sci. Eng.* **2000,** *28*, 1.
5. Zhu, Z. K.; Yang, Y.; Yin, J.; Wang, X. Y.; Ke, Y. C.; Qi, Z. N. *Polym. Chem.* **1999,** *31*, 2493.
6. Zanetti, M.; Kashiwagi, T.; Falqui, L.; Camino, G. *Chem. Mater.* **2002,** *14*, 881.
7. Schmidt, D.; Shah, D.; Giannelis, E. P. *Curr. Opin. Solid State Mater. Sci.* **2002,** *6*, 205.
8. Xie, W.; Xie, R.; Pan, W.; Hunter, D.; Koene, B.; Tan, L.; Vaia, R. *J. Chem. Mater.* **2002,** *14*, 4837.
9. Yoon, P. J.; Fornes, T. D.; Paul, D. R. *Polymer* **2002,** *43*, 6727.
10. Byrne, C.; McNally, T. *Macromol. Rapid Commun.* **2007,** *28*, 780.
11. Patel, H. A.; Somani, R. S.; Bajaj, H. C.; Jasra, R. V. *Appl. Clay Sci.* **2007,** *35*, 194.
12. Lebaron, P. C.; Wang, Z.; Pinnavaia, T. *Appl. Clay Sci.* **1999,** *15*, 11.
13. Mert, M.; Yilmazer, U. *J. Appl. Polym. Sci.* **2008,** *108*, 3890.
14. Giannelis, E. P. *Appl. Organomet. Chem.* **1998,** *12*, 675.
15. Mert, M.; Yilmazer, U. *Adv. Polym. Technol.* **2009,** *28*, 155.
16. Isik, I.; Yilmazer, U.; Bayram, G. *Polym. Compos.* **2008,** *29*, 133.
17. Coskunses, F.; Yilmazer, U. *J. Appl. Polym. Sci.* **2011,** *120*, 3087.
18. Favre, H.; Lagaly, G. *J. Clay Miner.* **1991,** *26*, 19.
19. Bergaya, F.; Lagaly, G. *Appl. Clay Sci.* **2001,** *19*, 1.
20. Gilman, J. W.; Awad, W. H.; Davis, R. D.; Shields, J.; Haris, R. H.; Davis, C., Jr.; Morgan, A. B.; Sutto, T. E.; Callahan, J.; Truvole, P. C.; DeLong, H. C. *Chem. Mater.* **2002,** *14*, 3776.
21. Awad, W. H.; Gilman, J. W.; Nyden, M.; Haris, R. H.; Sutto, T. E., Jr.; Callahan, J.; Truvole, P. C.; DeLong, H. C.; Fox, D. M. *Thermochim. Acta* **2004,** *409*, 3.
22. Calderon, J. U.; Lennox, B.; Kamal, M. R. *Appl. Clay Sci.* **2008,** *40*, 90.
23. Onal, M.; Sarikaya, Y.; Alemdaroglu, T.; Bozdogan, I. *Turk. J. Chem.* **2003,** *27*, 683.
24. Grim, R. E. Clay Mineralogy, 1st ed.; McGraw-Hill: New York, **1953.**
25. Abdallah, W.; Yilmazer, U. *Thermochim. Acta* **2011,** *525*, 129.
26. Awad, W. H.; Beyer, G.; Benderly, D.; Ijdo, W. L.; Songtipya, P.; Jimenez-Gasco, M. M.; Manias, E.; Wilkie, C. A. *Polymer* **2009,** *50*, 1857.
27. Qin, H.; Su, Q.; Zhang, S.; Zhao, B.; Yang, M. *Polymer* **2003,** *44*, 7533.
28. Kroschwitz, J. I.; Mark, H. F. Encyclopedia of Polymer Science and Technology, 3rd ed.; Wiley Interscience: Hoboken, NJ, **2003.**
29. Yu, Z. Z.; Yang, M.; Zhang, Q.; Zhao, C.; Mai, Y. W. *J. Polym. Sci. Part B: Polym. Phys.* **2003,** *41*, 1234.
30. Torok, B.; Bartok, M.; Dekany, I. *Colloid Polym. Sci.* **1999,** *277*, 340.
31. Hedley, C. B.; Yuan, G.; Theng, B. K. G. *Appl. Clay Sci.* **2007,** *35*, 180.
32. Han, B.; Ji, G.; Wu, S.; Shen, J. *Eur. Polym. J.* **2003,** *39*, 1641.
33. Cho, J. W.; Paul, D. R. *Polymer* **2001,** *42*, 1083.
34. Gonzales, I.; Eguiazabal, J. I.; Nazabal, J. *Polymer* **2005,** *46*, 2978.
35. Lee, K. M.; Han, C. D. *Macromolecules* **2003,** *36*, 7165.
36. Contreras, V.; Cafiero, M.; Da Silva, S.; Rosales, C.; Perera, R.; Matos, M. *Polym. Eng. Sci.* **2006,** *46*, 1111.
37. Vlasveld, D. P. N.; Vaidyaa, S. G.; Berseec, H. E. N.; Picken, S. J. *Polymer* **2005,** *46*, 3452.
38. Leszczynska, A.; Njuguna, J.; Pielichowski, K.; Banerjee, J. R. *Thermochim. Acta* **2007,** *453*, 75.
39. Zhang, Q. X.; Yu, Z. Z.; Yang, M.; Ma, J.; Mai, Y. W. *J. Polym. Sci. Part B: Polym. Phys.* **2003,** *41*, 2861.